J. Biochem. **139**, 733–740 (2006)
doi:10.1093/jb/mvj083

The Effect of Aβ Conformation on the Metal Affinity and Aggregation Mechanism Studied by Circular Dichroism Spectroscopy

Y.R. Chen[1], H.B. Huang[2], C.L. Chyan[3], M.S. Shiao[4], T.H. Lin[4,5,6,*] and Y.C. Chen[1,7,*]

[1]Institute of Medical Science, Tzu Chi University, Hualien, Taiwan; [2]Institute of Molecular Biology, National Chung-Cheng University, Chiayi, Taiwan; [3]Department of Chemistry, National Duan-Hwa University, Hualien, Taiwan; [4]Department of Medical Research and Education, Taipei Veterans General Hospital, Shihpai, Taipei, Taiwan; [5]Institute of Biochemistry and [6]Institute of Bioinformatics and Structural Biology Program, National Yang-Ming University, Shihpai, Taipei, Taiwan; and [7]Department of Medical Technology, Tzu Chi University, Hualien, Taiwan

Received January 11, 2006; accepted February 15, 2006

The conformational change and associated aggregation of β amyloid (Aβ) with or without metals is the main cause of Alzheimers' disease (AD). In order to further understand the effects of Aβ and its associated metals on the aggregation mechanism, the influence of Aβ conformation on the metal affinity and aggregation was investigated using circular dichroism (CD) spectroscopy. The Aβ conformation is dependent on pH and trifluoroethanol (TFE). The binding of metals to Aβ was found to be dependent on the Aβ conformation. The aggregation induced by Aβ itself or its associated metals is completely diminished for Aβ in 40% TFE. Only in 5% and 25% TFE can Aβ undergo an α-helix to β-sheet aggregation, which involve a three-state mechanism for the metal-free state, and a two-state transition for the metal-bound state, respectively. The aggregation-inducing activity of metals is in the order, $Cu^{2+} > Fe^{3+} \geqslant Al^{3+} > Zn^{2+}$.

Key words: Alzheimer's disease, β-amyloid (Aβ), conformational transition, circular dichroism spectroscopy.

Alzheimers' disease (AD) is a neurodegenerative disorder and the leading cause of senile dementia (*1*). One of the pathological hallmarks in AD patients is the formation of amyloid senile plaques (SPs) (*1*, *2*). The major components found in SPs are two small, hydrophobic peptide-amyloid β (Aβ) spanning residues 1–40 ($Aβ_{1–40}$) and 1–42 ($Aβ_{1–42}$), which are derived from a ubiquitous type I transmembrane protein–amyloid precursor protein (APP) by a two-step secretase pathway (*3–5*). The amyloid cascade hypothesis predicts that this β-amyloid plaque development in the brain has an early and essential role in the neuronal degeneration that leads to dementia (*1*, *2*).

The hypothesis that amyloid formation and deposition plays a key role in AD is supported by the observation that mutations which enhance the aggregation propensity of Aβ, such as dutch mutation (*6*), cause symptomatically severe early onset forms of AD. Fibrillogenesis has been proposed to be a two-step mechanism involving an initial slow, lag and nucleated period, followed by a rapid fibril propagation and aggregation stage (*7*). Peptide aggregation and precipitation were observed to occur following β-sheet formation by $Aβ_{1–39}$ and $Aβ_{1–42}$ in a time-dependent manner, indicating that formation of β-sheet structure is directly related to peptide aggregation (*8*, *9*).

The formation of Aβ fibers has been shown to be modulated by several factors, such as metal ions (*10*, *11*), pH (*12–14*), and interaction with other small molecules (*15–17*). Several cations, including Cu^{2+}, Zn^{2+}, Fe^{3+}, Fe^{2+} and Al^{3+}, have been reported to enhance the fibrillogensis of β-amyloid (*18–21*). The binding of Cu^{2+} and Fe^{3+} to Aβ has been linked to oxidative stress and toxicity (*22–25*). Metal chelators specific to Cu^{2+} and Zn^{2+} reverse the aggregation state (*26*, *27*). For pH effect, results from aggregation assay suggested that Aβ aggregates more rapidly at mildly acidic and neutral pH (*18*, *21*, *22*). When the pH of the peptide solution was decreased to between pH 1.0 and 3.0, the rate of fibril formation was decreased (*12*).

The Aβ aggregation cascade involves the conformation transition from random coil to β-sheet (*7–9*). Teplow and co-workers have proposed an alternate pathway, α-helix→β-sheet transition (*28*, *29*). Several *in vitro* studies of Aβ fibrillogensis have further indicated that the transition of structure from α-helix to β-sheet may play a prominent role in the amyloid fibril assembly (*30*, *31*). Paivio *et al.* (*32*) have proposed that many amyloid-forming proteins and peptides, including Aβ, contain α-helix/β-strand discordant sequences. Stabilizing the discordant helical conformation for Aβ has been proposed as a key factor for blocking fibril formation (*29*, *32–35*).

In the present study, we examined the effects of Aβ conformation on the affinity of metals to Aβ and on the aggregation mechanism using circular dichroism spectroscopy. We concluded that Aβ could adopt three distinct structures, "random coil," "unstable helix" and "stable helix," dependent on the concentration of TFE and pH. In the

*To whom correspondence should be addressed at: Department of Medical Technology, Tzu Chi University, Hualien 970, Taiwan. Fax: +886-3-8571917, E-mail: chen15@mail.tcu.edu.tw (Y.C. Chen); Department of Medical Research & Education, Taipei Veterans General Hospital, Teipei, Taiwan. E-mail: thlin@vghtpe.gov.tw (T.H. Lin).

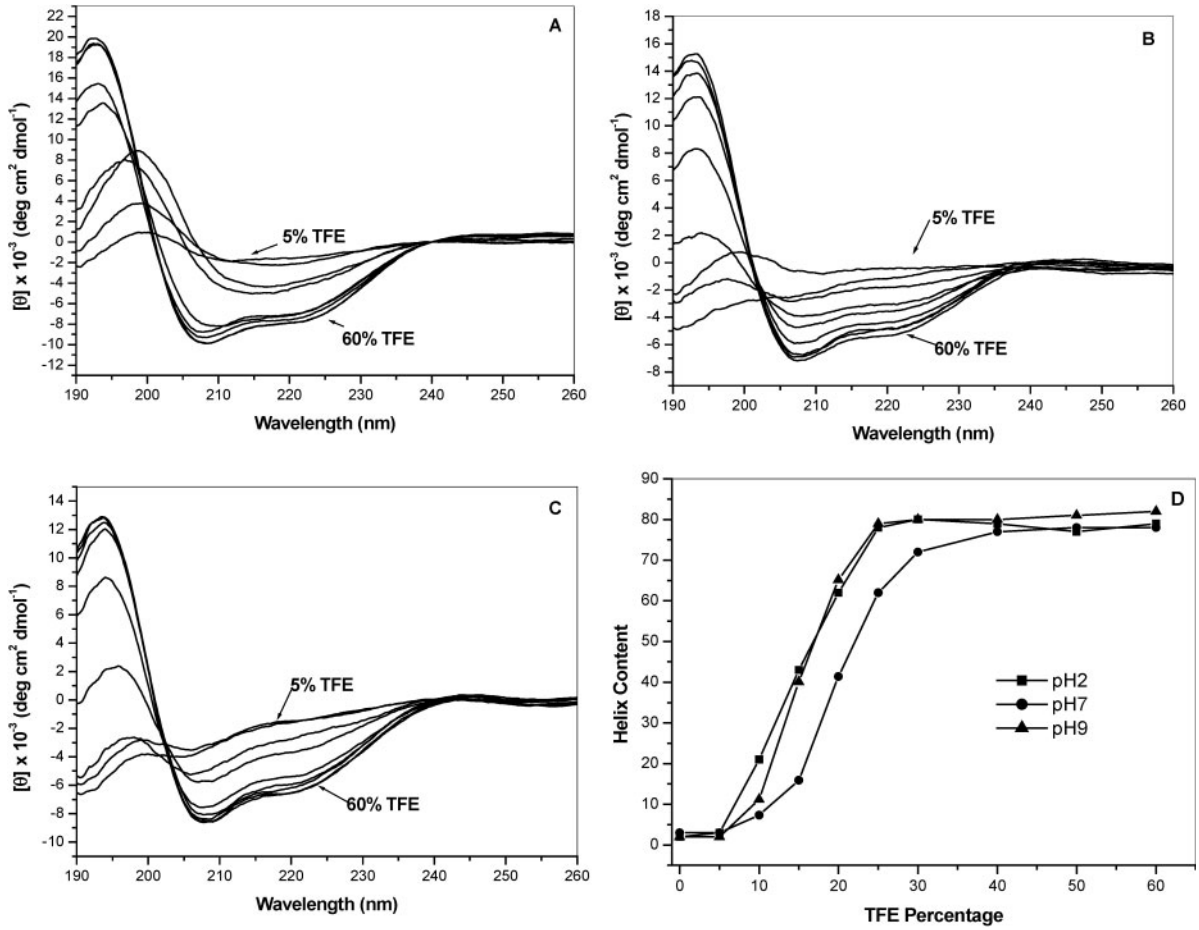

Fig. 1. **Far-ultralviolet circular dichroism spectra of β-amyloid, showing the titration with different percentages of TFE at (A) pH 2.0, (B) pH 7.0 and (C) pH 9.0.** In (A), (B) and (C), the TFE percentage was 5% (uppermost spectrum), 10%, 15%, 20%, 25%, 30%, 40%, 50% and 60% (lowermost spectrum). The concentration of Aβ used in the experiment was 50 μM. (D) Plot of CD signal at 222 nm *vs.* TFE percentage at pH 2.0 (squares), pH 7.0 (circles), and pH 9.0 (triangles).

"random coil" and "unstable helix" states, Aβ both in the metal-free and metal-bound states underwent a conformation-associated aggregation, while no aggregation was observed for Aβ in the "stable helix" state. This conformational transition associated aggregation showed a three-state mechanism for metal-free Aβ. On the other hand, when metals are bound to Aβ, the conformation underwent a two-state transition. The aggregation-inducing activity of metals is in the order $Cu^{2+} > Fe^{3+} \geqslant Al^{3+} > Zn^{2+}$.

MATERIAL AND METHODS

Peptide Synthesis and Purification—β-amyloid (Aβ) was synthsized in an ABI 433A solid-phase peptide synthesizer following the standard protocol. Cleavage and deprotection of the synthesized peptide were performed by treatment with a mixture of trifluoroacetic acid/distilled water/phenol/thioanisole/ethanedithiol. Then the peptide was extracted with 1:1 (v:v) ether:H_2O containing 0.1% 2-mercaptoethanol. The synthesized $A\beta_{1-40}$ was purified on a reverse-phase C-18 HPLC with a linear gradient from 40% to 100% acetonitrile, and its molecular weight was verified as 4330.1 by a MALDI-TOF mass spectroscopy (ABI).

Sample Preparation—A stock solution of 500 μM $A\beta_{1-40}$ was prepared. The stock solution was then diluted to the final concentration of 50 μM $A\beta_{1-40}$ in 100 mM glycine buffer with pH 1–10 containing 0–60% TFE for spectroscopic measurements. For the metal ion-induced effect on Aβ conformation, stock solutions containing Al^{3+}, Cu^{2+}, Fe^{3+} and Zn^{2+} ions were mixed with $A\beta_{1-40}$ stock solution to make the final concentration of 50 μM $A\beta_{1-40}$ and 100 μM metal ion in either 10 mM acetate buffer or 10 mM Tris buffer containing 25% TFE at pH 2.0, 7.0 and 9.0.

Circular Dichrosim (CD) Spectroscopy—CD spectra were recorded using a Jasco 715 spectropolarimeter with a thermal circulator accessory. The optical rotation was calibrated using *d*-10-camphorsulfonic acid at wavelengths of 192.5 and 290 nm. The wavelength was calibrated with benzene vapor. All measurements were performed in quartz cells with pathlength of 0.1 cm. Data were collected at the wavelengths from 190 to 260 nm in 0.2 nm increments. Every CD spectrum reported in the average obtained from at least three individual samples. The reported CD spectra were corrected for baseline using the solution containing 0–60% trifluoroethanol and the same concentration of

metal ion. All measurements were carried out at 25.0 ± 0.2°C.

Analysis of Secondary Structure—Secondary structure analysis was performed in an online web sever: Dicroweb (*36*, *37*). CDSSTR program (*38*) was used to estimate the related secondary structure. A normalized root mean standard deviation (NRMSD) (*39*) was applied to indicate the quality of fit for each spectrum, such that:

$$\mathrm{NRMSD} = [(\theta_{obs}(\lambda)-\theta_{cal}(\lambda))^2/(\theta_{obs}(\lambda))^2]^{1/2}$$

where $\theta_{obs}(\lambda)$ and $\theta_{cal}(\lambda)$ are the observed and calculated ellipticities, respectively. A low value for NRMSD suggests a good correspondence between the calculated values and the experimental data.

Kinetic Analysis—Kinetic data obtained from spectroscopic measurements were fitted using the non-linear curve-fitting program Micro Origin v.6.0 (Microcal Software, Inc. Northampton, MA). One or multiple exponential-phase algorithm was used to calculate the related rate constants. In the initial fitting stage, the Simplex method was used to calculate the initial input parameters to set up the rough parameter region. Then these parameters were used as constraints for further non-linear curve fitting. A 0.95 confidence level target was set to constrain the quality of the curve fitting. The final fitting parameters were obtained when the value of χ^2 was less than 0.05, and the parameters and the errors for the parameters reached a convergent and steady state.

RESULTS

Characterization of Aβ Conformation with Respect to pH and TFE—To investigate the effect of Aβ conformation on the Aβ aggregation mechanism, we first characterized the structure state of metal-free Aβ at different pHs and different proportions of TFE. CD spectra for Aβ in 100 mM glycine buffer at pH 2.0, 7.0 and 9.0 and with varying percentages of TFE are shown in Fig. 1, A, B and C, respectively. In general, increasing TFE concentration resulted in a conformational transition to a highly helical structure at all pH values. Figure 1D shows the relationship between helical content and TFE percentage at pH 2.0, 7.0 and 9.0. At pH 2.0 and 9.0, Aβ formed a stable α-helix at TFE ⩾ 30%, whereas at pH 7.0, Aβ adopted a stable helical structure at TFE ⩾ 40%.

Figure 2, A, B and C, shows the plots of secondary structure content versus pH for metal-free Aβ in 5%, 25% and 40% TFE, respectively. The values of NRMSD for all secondary structure analyses are within 0.08. The calculated and experimental CD spectra are in good fit. In 5% TFE, Aβ adopted the most random coil structure (~61%), whereas Aβ formed a stable helices (~77%) in 40% TFE. In both structural states, Aβ conformation is independent of pH. By contrast, in 25% TFE, Aβ conformation was pH-dependent and classified into two distinct states at pH 5.0–7.0 and other pH range (Fig. 2B). At pH other than 5.0–7.0, Aβ adopted mainly ~77% helical structure, whereas at pH 5.0–7.0, a ~77→62% decrease in helical content was associated with a ~10→20% increase in β-sheet content compared to the result obtained at other pH values.

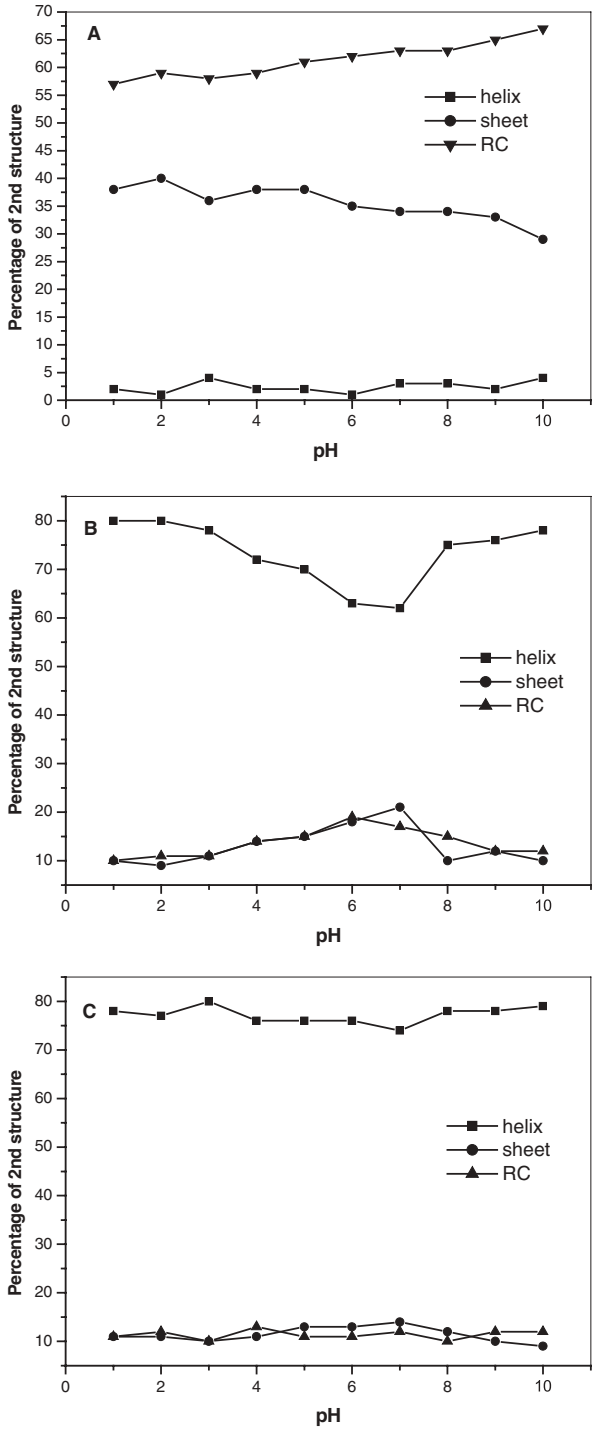

Fig. 2. **Plot of secondary structure percentage *vs.* pH for metal-free Aβ in solution containing (A) 5% TFE, (B) 25% TFE and (C) 40% TFE.** The concentration of Aβ was 50 μM. Secondary structure analysis was done using CDSSTR program in Dicroweb website. The changes of secondary structure with pH at 5% and 40% TFE are not obvious, while a significant decrease in α-helix at pH 5.0–7.0 can be observed in 25% TFE.

Aβ Conformation under the Effect of Metals—Metal ions have been proved to have an important effect on Aβ conformation and aggregation (*10*, *11*). Therefore, we examined the effect of Zn^{2+}, Al^{3+}, Fe^{3+}, and Cu^{2+} on Aβ

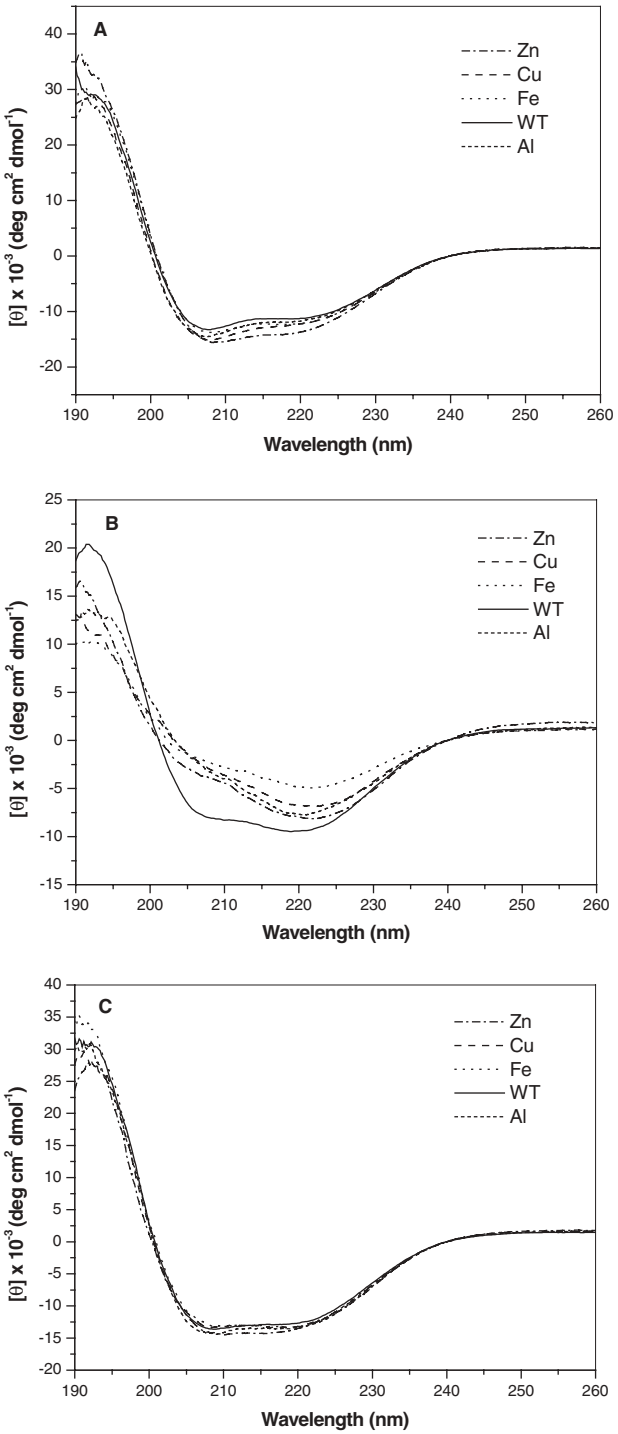

Fig. 3. **Far-ultraviolet circular dichroism spectra for metal-free Aβ (—), Cu^{2+}- (—), Fe^{3+}- (····), Zn^{2+}- (---), and Al^{3+}- (····) bound Aβ in (A) pH 2.0, (B) pH 7.0 and (C) pH 9.0 buffer containing 25% TFE.** In the experiments, the concentration of Aβ was 50 μM, and that of all metals was 100μM in order to make sure metals bound to Aβ. The intensity changes at 208 nm are more significant than that at 220 nm.

conformation in 5%, 25% and 40% TFE and at various pHs. CD spectra of Aβ with various metals in 25% TFE/ buffer, pH 2.0, 7.0, and 9.0 and at 0 h are depicted in Fig. 3, A, B and C, respectively. The CD spectral features at pH 7.0 (Fig. 3B) were clearly different from those obtained at pH 2.0 and 9.0. The intensity and pattern of CD spectra at pH 7.0 showed a decrease both at 220 and 208 nm compared to the metal-free states, whereas at pH 2.0 and 9.0 (Fig. 3, A and C), CD spectra for most metal ions showed no apparent change. Unlike the condition in 25% TFE, in 5% TFE, the CD spectra for Aβ in the presence of metals at all pH values showed a significant change from the features obtained in 25% TFE and at pH 7.0. By contrast, the CD spectral features measured in 40% TFE showed a highly helical content and were not altered by adding metals at any pH.

In 25% TFE and at pH 7.0, the secondary structure of Aβ in the presence of metals consisted of 11% α-helix, 35% β-sheet and 54% random coil. In comparison with metal-free Aβ under the same conditions, the α-helical content further decreased by 51% with an increase of 15% and 36% for β-sheet and random coil, respectively. The structural content with different metal ions showed no marked difference.

The Aβ Aggregation Mechanism with and without Metals—Based on the previous results, we further investigated the aggregation mechanism for Aβ with and without metals in 25% TFE and at pH 7.0. Figure 4A shows the CD spectra for metal-free Aβ versus times in 25% TFE solution, pH 7.0. An aggregation associated with the conformational transition from α-helix to β-sheet was clearly observed as the time increased. The CD spectral change at 208 nm was more significant than that at 220 nm (inset in Fig. 4A). Therefore, we used the intensity at 208 nm to estimate the rate of aggregation associated with conformational transition. Figure 4B shows the plot of intensity at 208 nm *versus* time for metal-free Aβ at pH 7.0. It can be seen that the signal reached a steady state after about 20 h. A two-phase exponential mode showed a better fit than a one-phase exponential mode, suggesting that metal-free Aβ undergoes a three-state mechanism. The estimated rate constants were 0.18 ± 0.05 h^{-1} for k_1 and 0.08 ± 0.02 h^{-1} for k_2. At pH 2.0 and 9.0, no signal change was detected even after 88 h (inset in Fig. 4B). This indicates that Aβ conformation was not changed or underwent an extremely slow aggregation at this pH.

As with the metal-free state, CD spectral change at 208 nm was used to monitor the conformational transition and aggregation rate for Aβ in the presence of metal ions. The plots of intensity at 208 nm versus time in 25% TFE solution with various metals, pH 7.0, are shown in Fig. 5, A, B, C, and D, for Zn^{2+}, Al^{3+}, Fe^{3+}, and Cu^{2+}, respectively. Unlike the metal-free state, the process of aggregation (or β-sheet formation) was best described by a one-phase exponential algorithm. All solid lines in figures represent the best fitting curves using the one-phase exponential algorithm. The estimated rate constants are listed in Table 1. All rate constants are in the range of 1.75–0.8 h^{-1}. In comparison with the rate constants for metal-free Aβ, result suggests that all metal ions significantly induced the aggregation of Aβ (or the transition of Aβ conformation) at pH 7.0. Both for metal-free and metal-associated Aβ, no aggregation (or conformational transition) at pH 2.0 and 9.0 could be detected within 88 h. The activity of metals to induce aggregation of Aβ as estimated from the aggregation assay is in the order $Cu^{2+} > Fe^{3+} \geqslant Al^{3+} > Zn^{2+}$. The rate by Cu^{2+} ions

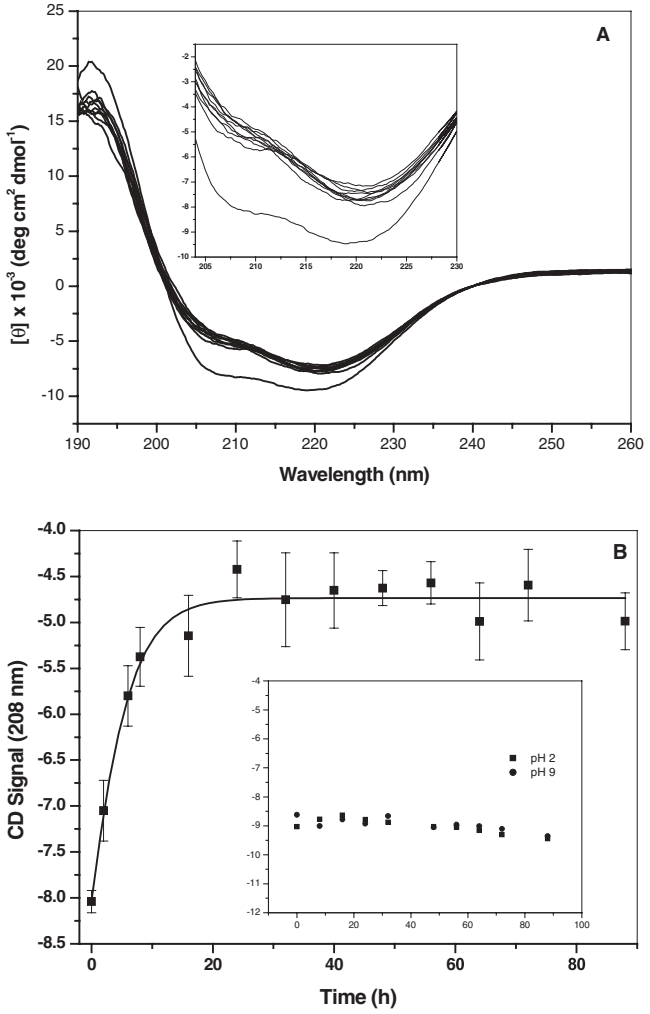

Fig. 4. **(A) Circular dichroism spectra of metal-free Aβ at 25% TFE and pH 7.0.** The lowermost CD spectrum is measured at 0 h. Inset shows the spectra at 200–220 nm. **(B) The plot of CD signal at 208 nm *vs.* time for metal-free Aβ under the same conditions as in (A).** In (B), the solid curve represents the non-linear curve fitting result using two-phase exponential algorithm, resulting in a three-state mechanism. Inset shows the same plot at pH 2.0 and pH 9.0 at pH 2.0 and pH 9.0, no transition of Aβ conformation is observed.

(1.75 ± 0.63 h^{-1}) is nearly 2.5-fold faster than the rate induced by Zn^{2+} ions (0.77 ± 0.09 h^{-1}) at pH 7.0.

DISCUSSION

In the present study, the metal-free Aβ was found to form different structural states under the effects of TFE and pH. These structural states show different properties associated with metal binding and aggregation mechanism. According to these different properties, the Aβ structural state can be classified into three categories: a pH-independent "random coil" structure at low TFE concentration (TFE < 5%), a pH-dependent "unstable helical" structure at intermediate TFE concentration (5% < TFE < 40%), and a pH-independent "stable helical" structure at high TFE concentration (TFE > 40%). In the stable helical state, Aβ maintains a high helical content and shows apparently no α-helix→β-sheet transition and aggregation with or without metals. In the random coil state, Aβ adopts a predominantly disordered structure and undergoes a rapid random coil→β-sheet transition and thereafter aggregation as proposed in the traditional Aβ aggregation cascade (*7–9*). Unlike the "random coil" state, the conformation of Aβ in the unstable helix state exhibits pH dependency. Only at pH 5.0–7.0 does Aβ show the conformational transition and aggregation.

Results obtained from the metal-induced Aβ conformational transition are similar to the metal-free state. Metals can induce Aβ conformational transition or aggregation only in the "random coil" and "unstable helix" states. In the "stable helix" state, the metal-mediated Aβ conformational transition and aggregation are completely diminished. In the "unstable helix" state, the metal-induced Aβ conformation shows significant transition and aggregation only at pH $\leqslant$ 9.0. At pH above 9.0, as in the "stable helix" state, the metal-driven conformational transition was not observed. Unlike the results observed in the stable helix and unstable helix states, the conformation of metal-bound Aβ in the "random coil" state underwent changes and aggregation over the whole pH range. This implies that the metal-induced conformational transition or aggregation is highly dependent on the Aβ structural states.

The Aβ aggregation process in the pH-dependent "unstable helix" state without metals undergoes a three-state conformational transition mechanism, α-helix→intermediate→β-sheet (aggregation state), with two rate constants, k_1 and k_2, applying to step1 and step2, respectively. With rate constants in the range of 10^{-1}–10^{-2} h^{-1}, these two transition steps undergo a slow transition process. k_1 is 2-fold faster than k_2. This indicates that the conversion from intermediate to β-sheet (aggregation state) in the second step is the rate-determining step in the transition process. Recently, a modeling study of the α-helix to β-strand transition mechanism of $A\beta_{12-28}$ showed that the transition involves the formation of an intermediate through a hydrophobic interaction (*40*). This Aβ intermediate was predicted to adopt a β-bend conformation with a loop at residues 20–24. In the present study, we provided the first experimental evidence for the existence of this intermediate.

Unlike the metal-free Aβ, the metal-bound Aβ undergoes a simple two-state mechanism, α-helix→β-sheet (aggregation state), and induces an even more significant conformational transition. The differences between these two mechanisms, particularly the lack of an intermediate in the metal-bound state, may be explained by two possible reasons. Firstly, the α-helix→β-sheet aggregation mechanism induced by metals is fast; for example, the transition rate of copper is 10-fold faster than the k_1 in metal-free state. Therefore, it may not be possible to detect the existence of intermediate in the measured time scale. Secondly, the metals bound to Aβ may be able to shift the Aβ conformation toward the disordered or β-sheet structure and, therefore, reduce the energy barrier and skip the formation of the intermediate. This is supported by EPR and Raman spectroscopic studies showing that the geometry of metal-His coordination center should be square-planer or square-pyramidal, and this shifts and distorts the whole conformation of copper-Aβ complex toward a random coil

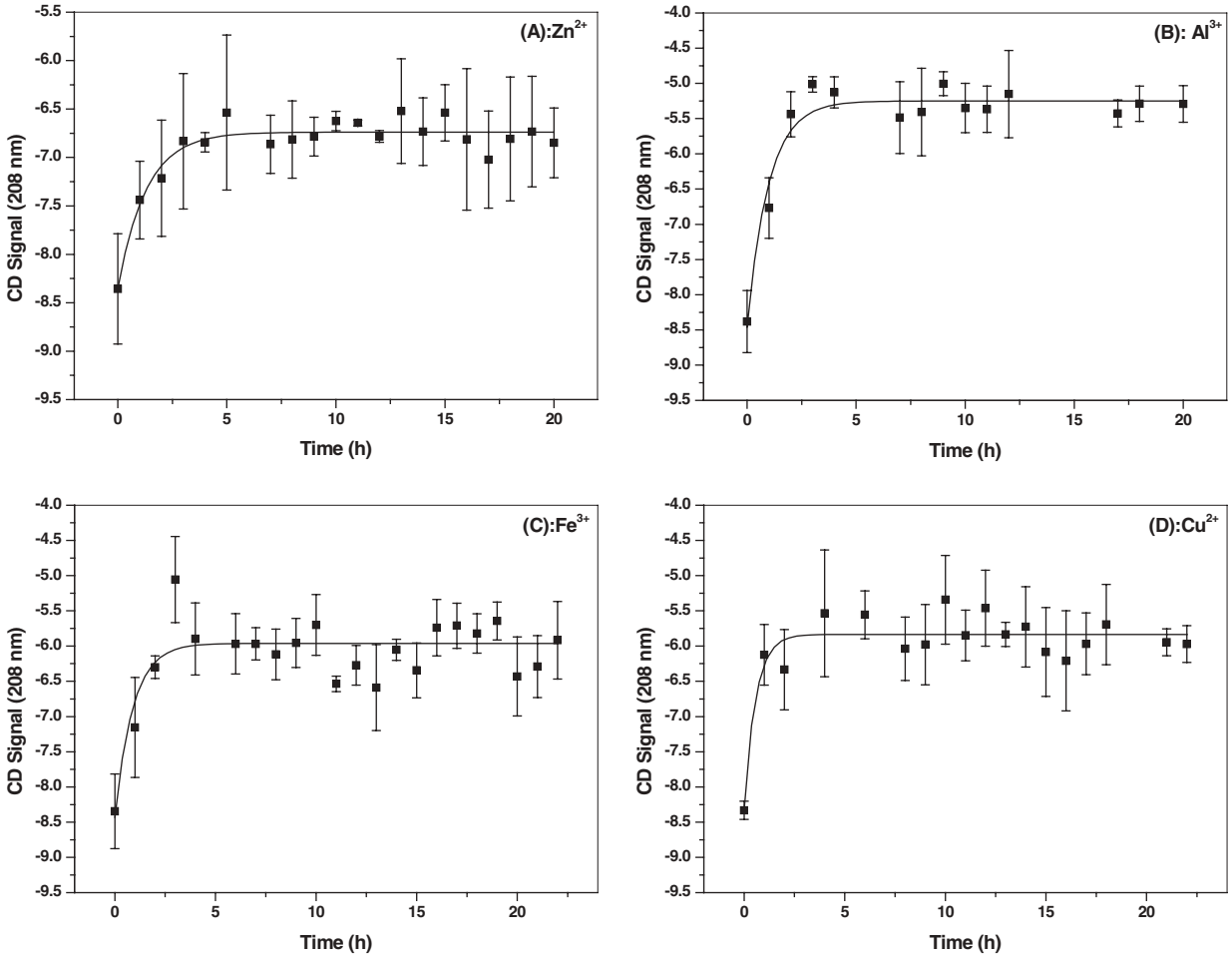

Fig. 5. **Plot of metal-bound Aβ conformation change rate as a function of CD signal at 208 nm *vs.* time for (A) Zn^{2+}, (B) Al^{3+}, (C) Fe^{3+}, and (D) Cu^{2+}.** The solid curves represent the best non-linear curve-fitting result for each metal ion using a one-phase exponential algorithm. It can be seen that copper induces the most effective transition in Aβ conformation, while zinc shows the smallest effect. A two-state model best represents the mechanism.

Table 1. **Calculated transition rate for Aβ induced by different metal ions.**

Metal ion	Rate (h^{-1})
Cu^{2+}	1.75 ± 0.63
Fe^{3+}	1.01 ± 0.52
Al^{3+}	1.01 ± 0.17
Zn^{2+}	0.77 ± 0.13

structure, particularly at the N-terminus (*40*, *41*). It is well characterized that the main metal binding region in Aβ is located at His^{13} and His^{14} residues, which is very near the discordant helical region ($K^{16}LVFFAED^{23}$) (*41–43*). Therefore, the binding of metals to these two histidine residues could change the microenvironment and destabilize the discordant helices, driving the conformation into β-sheet.

Furthermore, the formation of the "unstable helix" state in 25% TFE and "stable helix" state in 40% TFE for Aβ under the effect of metal, TFE and pH may reveal that the fine structures of Aβ are different in these structural states. From NMR studies of solution structures for Aβ in the solutions containing a high percentage of fluorinated alcohols, this "stable helical" Aβ is composed of two helical regions at the N- and C-terminus, connected by a β-turn or kink region centered on residues 24–28 (*44–46*). Therefore, Aβ in the "stable helix" state may form a stable helical structure with strongly residual interactions. This helical conformation is an energetically favorable structure and cannot easily be changed to other secondary structures by other factors. In contrast, in the "unstable helix" state, the Aβ conformation may be predominated by some forms of unstable helix with weakly residual interactions. This conformational state is energetically unfavorable, and can easily be changed by pH and metals. Recently, a discordant helical region located in Aβ residues 16–23 has been proposed (*32*, *43*). Our present concept of "unstable helix" state may be correlated with this discordant helices hypothesis. However, the detailed differences between these two structural states need to be further characterized.

In summary, the Aβ under the effects of TFE and pH could form three structural states, "random coil," "unstable

helix" and "stable helix." The characterization of Aβ conformational transition and aggregation is highly dependent on the nature of these structural states. The aggregation processes for metal-free and metal-bound Aβ in the "unstable helix" state involves different mechanisms, three-state for the metal-free state and two-state for the metal-bound state.

This work was supported by grants from National Science Council of Taiwan, R.O.C. (NSC 912113M320-001 to Y.C.C.), Tzu Chi University (TCMR93007 to Y.C.C.) and (NSC932311B010-010 to T.H.L.)

REFERENCES

1. Selkoe, D.J. (1991) The molecular pathology of Alzheimer's disease. *Neuron* **6**, 487–498
2. Skovronsky, D.M., Doms, R.W., and Lee, V.M. (1998) Detection of a novel intraneuronal pool of insoluble amyloid beta protein that accumulates with time in culture. *J. Cell. Biol.* **141**, 1031–1039
3. Tanzi, R.E., Bird, E.D., Latt, S.A., and Neve, R.L. (1987) The amyloid beta protein gene is not duplicated in brains from patients with Alzheimer's disease. *Science* **238**, 666–669
4. Kang, J., Lemaire, H.G., Unterbeck, A., Salbaum, J.M., Masters, C.L., Grzeschik, K.H., Multhaup, G., Beyreuther, K., and Muller-Hill, B. (1987) The precursor of Alzheimer's disease amyloid A4 protein resembles a cell-surface receptor. *Nature* **325**, 733–736
5. Haass, C. Huang, A.Y., Schlossmacher, M.G., D., Teplow, D.B., and Selkoe, D.J. (1993) beta-Amyloid peptide and a 3-kDa fragment are derived by distinct cellular mechanisms. *J. Biol. Chem.* **268**, 3021–3024
6. Levy, E., Carman, M.D., Fernandez-Madrid, I.J., Power, M.D., Lieberburg, I., van Duinen, S.G., Bots, G.. T., Luyendijk, W., and Frangione, B. (1990) Mutation of the Alzheimer's disease amyloid gene in hereditary cerebral hemorrhage, Dutch type. *Science* **248**, 1124–1126
7. Lomakin, A., Chung, D.S., Benedek, G.B., Kirschner, D.A., and Teplow, D.B. (1996) The role of APP processing and trafficking pathways in the formation of amyloid beta-protein. *Proc. Natl. Acad. Sci. USA* **93**, 1125–1129
8. Barrow, C.J., Yasuda, A., Kenny, P.T., and Zagorski, M.G. (1992) Solution conformations and aggregational properties of synthetic amyloid beta-peptides of Alzheimer's disease. Analysis of circular dichroism spectra. *J. Mol. Biol.* **225**, 1075–1093
9. Serpell, L.C. and Smith, J.M. (2000) Direct visualisation of the beta-sheet structure of synthetic Alzheimer's amyloid. *J. Mol. Biol.* **299**, 225–231
10. Atwood, C.S., Moir, R.D., Huang, X., Scarpa, R.C., Bacarra, N.M., Romano, D.M., Hartshorn, M.A., Tanzi, R.E., and Bush, A.I. (1998) Dramatic aggregation of Alzheimer abeta by Cu(II) is induced by conditions representing physiological acidosis. J. Biol. Chem. **273**, 12817–12826
11. Bush, A.I., Multhaup G., Moir, R.D., Williamson, T.G., Small, D.H., Rumble, B., Pollwein, P., Beyreuther, K., and Masters, C.L. (1993) A novel zinc(II) binding site modulates the function of the beta A4 amyloid protein precursor of Alzheimer's disease. *J. Biol. Chem.* **268**, 16109–16112
12. Zagorski, M.G. and Barrow, C.J. (1992) NMR studies of amyloid beta-peptides: proton assignments, secondary structure, and mechanism of an alpha-helix—beta-sheet conversion for a homologous, 28-residue, N-terminal fragment. *Biochemistry* **31**, 5621–5631
13. Zagorski, M.G., Yang, J., Shao, H., Ma, K., Zeng, H., and Hong, A. (1999) Methodological and chemical factors affecting amyloid beta peptide amyloidogenicity. *Methods Enzymol.* **309**, 189–204
14. Matsunaga, Y., Saito, N., Fuji, A., Yokotani, J., Takakura, T., Nishimura, T., Esaki, H., and Yamada, T. (2002) A pH-dependent conformational transition of Abeta peptide and physicochemical properties of the conformers in the glial cell. *Biochem. J.* **361**, 547–556
15. Soto, C., Castano, E.M., Kumar, R.A., Beavis, R.C., and Frangione, B. (1995) Fibrillogenesis of synthetic amyloid-beta peptides is dependent on their initial secondary structure. *Neurosci. Lett.* **200**, 105–108
16. Soto, C., Castano, E.M., Prelli, F., Kumar, R.A., and Baumann, M. (1995) Apolipoprotein E increases the fibrillogenic potential of synthetic peptides derived from Alzheimer's, gelsolin and AA amyloids. *FEBS Lett.* **371**, 110–114
17. Evans, K.C., Berger, E.P., Cho, C.G., Weisgraber, K.H., and Lansbury, P.T. Jr. (1995) Apolipoprotein E is a kinetic but not a thermodynamic inhibitor of amyloid formation: implications for the pathogenesis and treatment of Alzheimer disease. *Proc. Natl. Acad. Sci. USA* **92**, 763–767
18. Atwood, C.S., Scarpa, R.C., Huang, X., Moir, R.D., Jones, W.D., Fairlie, D.P., Tanzi, R.E., and Bush, A.I. (2000) Characterization of copper interactions with alzheimer amyloid beta peptides: identification of an attomolar-affinity copper binding site on amyloid beta1-42. *J. Neurochem.* **75**, 1219–1233
19. Bush, A.I., Pettingell, W.H. Jr., Multhaup, G.., Paradis, M.D., Vonsattel, J.P., Gusella, J.F., Beyreuther, K., Masters, C.L., and Tanzi, R.E. (1994) Rapid induction of Alzheimer A beta amyloid formation by zinc. *Science* **265**, 1464–1467
20. Manthy, P.W., Ghilardi, J.R. , Rogers, S., DeMaster ,E., Allen, C.J., Stimson, E.R., and Maggio, J.E. (1993) Aluminum, iron, and zinc ions promote aggregation of physiological concentrations of beta-amyloid peptide. *J. Neurochem.* **61**, 1171–1174
21. Good, P.F., Perl, D.P., Bierer L.M., and Schmeidler, J. (1992) Selective accumulation of aluminum and iron in the neurofibrillary tangles of Alzheimer's disease: a laser microprobe (LAMMA) study. *Ann. Neurol.* **31**, 286–292
22. He, W. and Barrow, C.J. (1999) The A beta 3-pyroglutamyl and 11-pyroglutamyl peptides found in senile plaque have greater beta-sheet forming and aggregation propensities in vitro than full-length A beta. *Biochemistry* **38**, 10871–10877
23. Cardoso, S.M., Santana, I., Swerdlow, R.H., and Oliveira, C.R. (2004) Mitochondria dysfunction of Alzheimer's disease cybrids enhances Abeta toxicity. *J. Neurochem.* **89**, 1417–1426
24. Huang, X., Moir, R.D., Tanzi, R.E., Bush, A.I., and Rogers, J.T. (2004) Redox-active metals, oxidative stress, and Alzheimer's disease pathology. *Ann. N.Y. Acad. Sci.* **1012**, 153–163
25. Lynch, T., Cherny, R.A., and Bush, A.I. (2000) Oxidative processes in Alzheimer's disease: the role of abeta-metal interactions. *Exp. Gerontol.* **35**, 445–451
26. Huang, X., Atwood, C.S., Moir, R.D., Hartsborn, M.A., Vonsattel, J.P., Tanzi, R.E., and Bush, A.I. (1997) Zinc-induced Alzheimer's Abeta1-40 aggregation is mediated by conformational factors. *J. Biol. Chem.* **272**, 26464–26470
27. Cherny, R.A., Legg, J.T., McLean, C.A., Fairlie, D.P., Huang, X., Atwood, C.S., Beyreuther, K., Tanzi, R.E., Masters, C.L., and Bush, A.I. (1999) Aqueous dissolution of Alzheimer's disease Abeta amyloid deposits by biometal depletion. *J. Biol. Chem.* **274**, 23223–23228
28. Kirkitadze, M.D., Condron, M.M., and Teplow, D.B. (2001) Identification and characterization of key kinetic intermediates in amyloid beta-protein fibrillogenesis. *J. Mol. Biol.* **312**, 1103–1119
29. Fezoui, Y. and Teplow, D.B. (2002) Kinetic studies of amyloid beta-protein fibril assembly. Differential effects of alpha-helix stabilization. *J. Biol. Chem.* **277**, 36948–36954
30. Walsh, D.M., Lomakin, A., Benedek, G.B., Condron, M.M., and Teplow, D.B. (1997) Amyloid beta-protein fibrillogenesis.

Detection of a protofibrillar intermediate. *J. Biol. Chem.* **272**, 22364–22372
31. Walsh, D.M., Hartley, D.M., Kusumoto, Y., Fezoui, Y., Condron, M.M., Lomakin, A., Benedek, G.B., Selkoe, D.J., and Teplow, D.B. (1999) Amyloid beta-protein fibrillogenesis. Structure and biological activity of protofibrillar intermediates. *J. Biol. Chem.* **274**, 25945–25952
32. Paivio, A., Nordling, E., Kallberg, Y., Thyberg, J., and Johansson, J. (2004) Stabilization of discordant helices in amyloid fibril-forming proteins. *Protein Sci.* **13**, 1251–1259
33. Shanmugam, G. and Jayakumar, R. (2004) Structural analysis of amyloid beta peptide fragment (25–35) in different microenvironments. *Biopolymers* **76**, 421–434
34. D'Ursi, A.M., Armenante, M.R., Guerrini, R., Salvadori, S., Sorrentino, G., and Picone, D. (2004) Solution structure of amyloid beta-peptide (25–35) in different media. *J. Med. Chem.* **47**, 4231–4238
35. Tiana, G.., Simona, F., Broglia, R.A., and Colombo, G.. (2004) Thermodynamics of beta-amyloid fibril formation. *J. Chem. Phys*. **120**, 8307–8317
36. Whitmore, L. and Wallace, B.A. (2004) DICHROWEB, an online server for protein secondary structure analyses from circular dichroism spectroscopic data. *Nucleic Acids Res.* **32**, 668–673
37. Lobley, A., Whitmore, L., and Wallace, B.A. (2002) DICHROWEB: an interactive website for the analysis of protein secondary structure from circular dichroism spectra. *Bioinformatics* **18**, 211–212
38. Compton, L.A. and Johnson, W.C. Jr. (1986) Analysis of protein circular dichroism spectra for secondary structure using a simple matrix multiplication. *Anal. Biochem.* **155**, 155–167
39. Mao, D., Wachter, T.A., and Wallace, B.A. (1982) Folding of the mitochondrial proton adenosinetriphosphatase proteolipid channel in phospholipid vesicles. *Biochemistry* **21**, 4960–4968
40. Simona, F., Tiana, G., Broglia, R.A., and Colombo, G. (2004) Modeling the alpha-helix to beta-hairpin transition mechanism and the formation of oligomeric aggregates of the fibrillogenic peptide Abeta(12–28): insights from all-atom molecular dynamics simulations. *J. Mol. Graph. Mod.* **23**, 263–273
41. Syme, C.D., Nadal, R.C., Rigby, S.E., and Viles, J.H. (2004) Copper binding to the amyloid-beta (Abeta) peptide associated with Alzheimer's disease: folding, coordination geometry, pH dependence, stoichiometry, and affinity of Abeta-(1–28): insights from a range of complementary spectroscopic techniques. *J. Biol. Chem.* **279**, 18169–18177
42. Curtain C.C., Ali, F., Smith, D.G., Bush, A.I., Masters, C.L., and Barnham, K.J. (2003) Metal ions, pH, and cholesterol regulate the interactions of Alzheimer's disease amyloid-beta peptide with membrane lipid. *J. Biol. Chem.* **278**, 2977–2982
43. Soto, C., Castano, E.M., Frangione, B., and Inestrosa, N.C. (1995) The alpha-helical to beta-strand transition in the amino-terminal fragment of the amyloid beta-peptide modulates amyloid formation. *J. Biol. Chem.* **270**, 3063–3067
44. Bush, A.I., Pettingell, W.H. Jr., Paradis, M.D., and Tanzi, R.E. (1994) Modulation of A beta adhesiveness and secretase site cleavage by zinc. *J. Biol. Chem.* **269**, 12152–12158
45. Shao, H., Jao, S., Ma, K., and Zagorski, M.G. (1999) Solution structures of micelle-bound amyloid beta-(1–40) and beta-(1–42) peptides of Alzheimer's disease. *J. Mol. Biol.* **285**, 755–773
46. Crescenzi, O., Tomaselli, S., Guerrini, R., Salvadori, S., D'Ursi, A.M., Temussi, P.A., and Picone, D. (2002) Solution structure of the Alzheimer amyloid beta-peptide (1–42) in an apolar microenvironment. Similarity with a virus fusion domain. Eur. J. Biochem. **269**, 5642–5648